Effect of Two Endwall Contours on the Performance of an Annular Nozzle Cascade

S. H. Moustapha*
Pratt and Whitney Canada Inc., Longueuil, Quebec, Canada
and
R. G. Williamson†
National Research Council of Canada, Ottawa, Ontario, Canada

An annular nozzle cascade, of low aspect ratio and high flow turning, was tested with two different endwall contours over a range of exit flow conditions from subsonic to supersonic. Measurements were made of the distributions of exit total pressure and flow angle. Significant performance degradation occurred with increasing Mach number, particularly in the vicinity of the hub. Observed differences in radial loss distribution between the two nozzle builds were correlated with predicted static pressure differences on the endwalls.

Nomenclature

Cp_o = local total pressure loss coefficient $Pom_1 - Po_2/Pom_1 - Psm_2$
$\overline{Cp_o}$ = circumferential mean of Cp_o
$\overline{\overline{Cp_o}}$ = area weighted radial mean of $\overline{Cp_o}$
Cx = axial chord at midspan
Pom = mean total pressure
Po = local total pressure
PR = nozzle total to static pressure ratio Pom_1/Psm_2
Psm = mean static pressure
Ps = local static pressure
q = area weighted mean of $Po_2 - Ps_2$
Yp = area weighted mean of $Pom_1 - Po_2/Pom_1$
Yq = area weighted mean of $Pom_1 - Po_2/q$
α = local exit yaw angle (from axial)
$\bar{\alpha}$ = circumferential mean of α
$\bar{\bar{\alpha}}$ = area weighted radial mean of $\bar{\alpha}$

Subscripts

1 = nozzle inlet plane
2 = nozzle exit plane, 0.14 Cx from nozzle trailing edge

Introduction

TURBINE design requirements for the gas generator section of small aircraft engines are centered around the achievement of lightness, reliability, and high performance leading to the selection of single-stage axial turbines operating at relatively high pressure ratios and inlet temperatures.

The nozzle design for such a turbine will have twisted vanes with high flow turning, low aspect ratio, high exit Mach numbers, and large trailing-edge blockages to provide for effective cooling. These nozzle design features can combine to produce excessive secondary flows and losses which may seriously affect the performance of the subsequent high-work rotor. In the quest for methods of improving the performance of such nozzles, considerable attention has been paid to endwall contouring which offers the possibility of reducing exit flow profile distortion, as well as controlling secondary flow development, by reduction of cross-channel and radial static pressure gradients. In particular, contouring the endwall so as to effect a reduction in annulus height through the nozzle permits most of the flow turning to be achieved at lower velocities around the initial region of the vane. Subsequent additional flow acceleration is then available to reduce flow profile distortion and boundary layer growth. Confining the endwall contouring to the annulus tip offers the possibility of alleviating radial pressure gradients which tend to drive low momentum flow to the hub region.

The potential benefits of such a design feature were first reported by Deich et al.,[1] and subsequent work[2-9] has attempted to quantify the gains under conditions that incorporated varying degrees of realism. Kopper et al.[5] demonstrated a 17% loss reduction due to endwall contouring in tests conducted on a linear nozzle cascade with an aspect ratio of 0.5 and an exit Mach number of 0.85. A major part of the measured improvement resulted from a reduction of secondary loss on the planar wall side of the cascade. The effect of contouring on stator and stage performance was reported by NASA researchers[6-8] through experiments carried out on a lightly loaded annular nozzle (Zweifel coefficient 0.48) with near sonic exit conditions. These investigations showed that the improvement in stage efficiency due to contouring (about 0.5 to 0.8%) stemmed largely from reduced stator profile and endwall friction losses. It was recommended that the merit of endwall contouring in reducing secondary losses be verified in a more heavily loaded design. Recently, Boletis[9] described the effects of endwall contouring on the evolution of the three-dimensional flowfield in a low-speed annular nozzle cascade. Contouring was found to decrease the overall losses by about 15%.

The present work is part of an ongoing research program begun in the mid 1970s and aimed at furthering the understanding of the aerodynamics of highly loaded turbines. An experimental investigation was designed to compare the performance of two different endwall contours when applied to an annular nozzle with an aspect ratio of 0.6, nominal turning 76 deg, and Zweifel coefficient of 0.83. The nozzles were tested at several pressure ratios, corresponding to a mean exit Mach number range of 0.6 to 1.2.

Attention was directed initially toward establishing the aerodynamic performance of the two nozzle builds in the absence of a rotor. Recognizing that stage performance would be influenced by changes in radial distribution of loss

Received May 17, 1985; presented as Paper 85-1218 at the AIAA/ASME/SAE 21st Joint Propulsion Conference, Monterey, CA, July 8-10, 1985; revision received Nov. 26, 1985.

*Staff Aerodynamicist, Turbine Research and Design.
†Head, Gas Dynamics Laboratory.

and exit flow angle as well as their integrated magnitudes, it is planned to test both nozzle designs with a representative high work rotor to permit direct comparison of the influence of the two endwall contours on overall stage performance. It is also intended to investigate nozzle exit flow conditions with the rotor in place, allowing an assessment of rotor interaction effects on nozzle performance.

Nozzle Design

The nozzles used in the present investigation were designed for a highly loaded turbine stage, resulting in an aspect ratio of 0.6 (based on true chord), a turning angle of 76 deg, and an exit Mach number of 1.2 at the vane mean section. Compromise between the cooling requirements of a typical engine application, the aspect ratio dependent (secondary) losses, and the optimum airfoil loading fixed the number of vanes as 14. The vane section was chosen to accomplish most of the flow turning near the leading edge; induced incidence effects were considered in the leading edge design. Vane sections were stacked such that the trailing edge was straight and radial in meridional and axial views. Vane details are shown in Fig. 1.

Two endwall contours were tested. Each configuration used meridional wall profiling to effect a reduction in tip height from inlet to exit of 15%, a value close to the recommendations of Deich et al.[1] Nozzle C employed a conical contour from inlet to exit, while nozzle S used a more rapid S contour variation starting in the vicinity of the throat. Although the designs date from the mid 1970s, it is interesting to note the similarities between the present contour configurations and those evolved independently in Ref. 7. A meridional view of the stator, showing the two wall contours, is presented in Fig. 2. In order to maintain the same throat area between nozzle builds, it was necessary to re-stagger the S wall variant 0.72 deg closed compared to the C version.

A three-dimensional inviscid Euler flow solver (based on Ref. 10) was used to predict isentropic Mach number distributions on the vane and endwall surfaces at various pressure ratios. Figures 3 and 4 show vane Mach number distributions at hub and tip, respectively, for both nozzle builds at design pressure ratio. It is evident that although the results at the hub show generally similar trends for the two nozzles up to about 70% chord, the C variant incurs a slightly higher peak Mach number and consequently somewhat greater final diffusion. At the outer wall (Fig. 4) the effect of the S contour is to unload the suction surface of the vane, tending to reduce the cross-channel pressure gradient when compared to the C version.

Comparison of calculated static pressure distributions on the endwalls (Fig. 5) suggests broadly similar conditions for both nozzle designs, although two points are worth noting. At the tip a low pressure region (and subsequent adverse pressure gradient) associated with the rapid contour changes of the S wall is evident near the suction surface of the vane downstream of the throat. In the case of the hub endwalls, it is the C nozzle which shows the greater adverse pressure gradients near the exit, associated with the trailing edge shock system. The possible consequences of these static pressure distributions on the measured nozzle performance are discussed later.

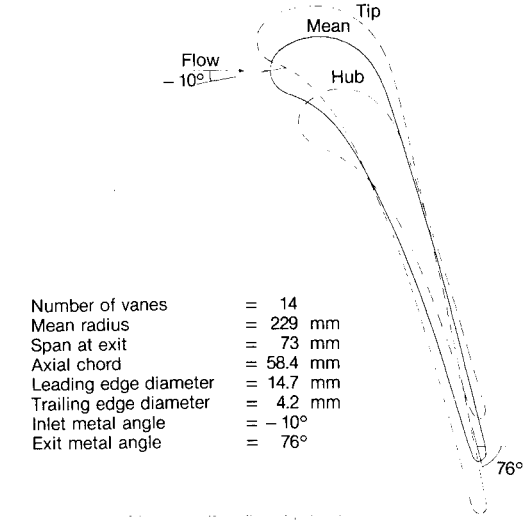

Fig. 1 Vane sections and midspan geometric parameters.

Experimental Arrangements

Test Details

The facility was designed to accommodate single turbine stages of about 53 cm o.d. with blade heights up to 7½ cm.

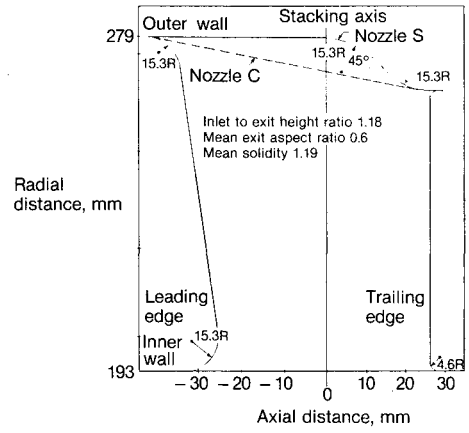

Fig. 2 Stator meridional view.

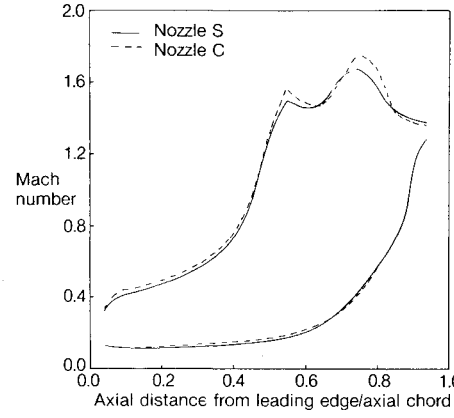

Fig. 3 Predicted vane hub Mach number distributions ($PR = 2.3$).

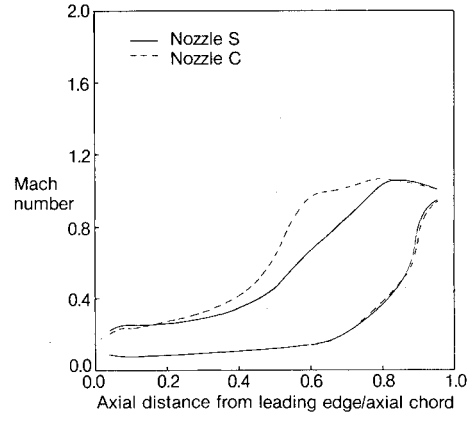

Fig. 4 Predicted vane tip Mach number distributions ($PR = 2.3$).

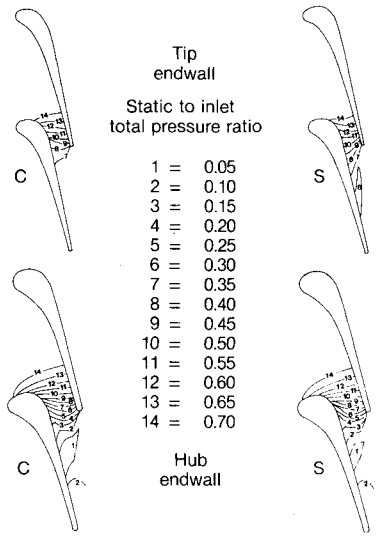

Fig. 5 Predicted endwall static pressure contours ($PR = 2.3$).

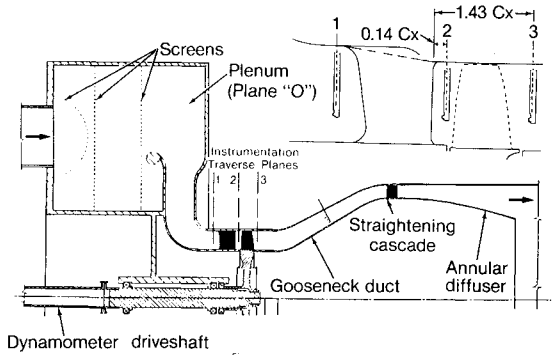

Fig. 6 The highly loaded turbine rig.

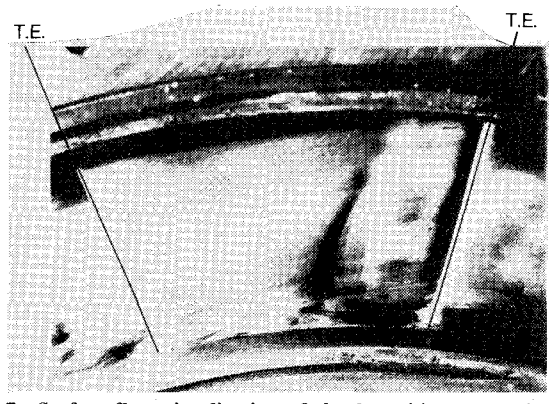

Fig. 7 Surface flow visualization of shock position on suction surface (view looking upstream, $PR = 2.3$).

Such dimensions are typically several times those of full size small turbine engines and permit "cold" testing at representative Mach and Reynolds numbers, with ample space for comprehensive instrumentation. A sketch of the overall layout, which also shows instrumentation planes, is presented in Fig. 6.

Air was drawn through the rig by a separate exhauster plant. In tests on a complete stage the inlet air can be prewarmed by mixing with the output of a propane combustor to maintain stage exit temperature near cell ambient conditions. The prewarming feature was used in the present series of tests on nozzles alone when ambient conditions of low temperature and/or high humidity would have led to freezing or condensation problems at nozzle exit. Inlet temperatures in these tests were limited to about 35°C.

For the present tests the rotor was replaced by a dummy ring of diameter equal to that of the rotor blade hub platform, as shown in Fig. 6. It is noted that small steps were present in outer and inner walls, corresponding to actual design practice associated with cooling requirements. For these tests conducted in the absence of a rotor, it was necessary to throttle the inlet slightly to permit the exhauster to operate within its power limitations. The plenum pressure was generally about 0.75 bar. Mass flow at design pressure ratio was 4.1 kg/s, corresponding to a mean inlet Mach number of 0.1. Vane Reynolds number based on mean chord and inlet conditions was about 1.8×10^6 and near 9×10^6 based on exit conditions.

Instrumentation

Instrumentation was designed to explore gas angles and pressures under steady-state conditions. Mass flow was measured by a calibrated bellmouth at entry to the mixing tank. Plenum conditions (plane 0) were sensed by 16 partially shielded thermocouples equispaced around the circumference and by four static pressure tappings. In view of the very low air velocities involved, the measurements were assumed to represent inlet stagnation conditions.

Nozzle inlet conditions (plane 1) were defined by three static pressure tappings at both hub and tip, and were explored in more detail by radial traverses at three locations approximately 90 deg apart, each circumferentially midway between adjacent vane leading edges at the tip surface.

The test facility permitted radial and circumferential traversing at the nominal nozzle exit plane. The actual traverse position was 8.5 mm axially downstream of the nozzle trailing edge (corresponding to 0.14 nozzle axial mean chords). Traverses were performed using a 4.8 mm diam wedge probe. Approach of the probe to the hub was limited by contact with the wall when the total pressure port was 4.8 mm from the surface. Considerable care was taken to ensure adequate sealing of the traverse slots, and final checks were made with smoke to ensure no detectable leaks were present.

The probe was operated under computer control, and was automatically nulled for flow direction at each preselected point before angle and pressure data were recorded. For each circumferential position, data were secured at 12 radial immersions of the probe. A total of 11 circumferential increments, equispaced across a nozzle exit, was required to complete the mapping for each test condition. Experiments were conducted at several nominal pressure ratios ranging from subsonic to supersonic exit conditions.

No attempt was made to derive local static pressure from probe readings in the complex high Mach number flow field of wakes and secondary flows. Analysis indicated a near linear mean static pressure gradient from hub to tip could be expected. Accordingly, linear interpolation from measured wall static pressures at the measurement planes was adopted in calculations of local Mach numbers. This was done without regard for local circumferential variations from blade to blade or variations in wakes and secondary flows. Nozzle exit wall static pressures were averaged from blade to blade at hub and tip by using circumferential slits which extended over two nozzle exit passages and which connected to relatively large volume subsurface chambers in which the static pressures were measured.

Traverse positional accuracy is estimated at ± 0.5 mm radially and ± 2 mm circumferentially. Accuracy in yaw was a function of flow conditions, more difficulty being experienced in nulling the probe in regions of unsteadiness associated with blade wakes and strong secondary flows. Although probe calibrations were repeatable to within ± 0.2 deg, repeatability in the more difficult exit flow regions was not better than ± 2 deg. It is noted, however, that the circumferentially averaged values of yaw angle were generally repeatable to within ± 0.8 deg.

Accuracy of surface static pressures is estimated as ±0.01 of total pressure. Values of Cp_o are considered accurate to within ±.01 in areas of relatively low total pressure loss. Some practical confirmation of this is provided by examination of data from the areas of the nozzle exit plane indicating a nominal zero loss. The two independently measured pressures (Pom_1 and the probe total pressure) agreed closely in these locations. Errors introduced by nulling the traverse probe in regions of large pressure gradients, and the fact that pitch angle error on probe total pressure measurement was neglected, were expected to cause additional uncertainties in a small proportion of the readings. Overall averages are affected by these errors and by the difficulties of the interpolation when averaging discrete values in rapidly changing total pressure gradients, such as blade wakes.

Experimental Results

Inlet Conditions

Inlet turbulence level at midannulus height was assessed using a constant temperature hot wire probe mounted at the inlet traverse location. The measured longitudinal intensity of 1.7% was independent of test Mach number and is probably low by actual turbine inlet standards.

Inlet traverses were conducted at the three circumferential positions using a cobra probe that permitted total pressure and angularity readings to be obtained near to the annulus walls. Typical inlet velocity profiles were seen to be essentially flat with thin boundary layers, particularly at the hub. Boundary layer thicknesses in terms of annulus height are estimated as 2% at hub and 9% at tip. Measured flow angularity was less than 10 deg from axial and was clearly affected by nearby vane leading edges which were not radial (in either circumferential or meridional planes), and whose proximity was therefore a function of probe immersion.

Wall Pressure Distributions and Flow Visualization

In order to provide a check on analytical methods for calculation of surface Mach number distributions in the nozzles, it had been decided to instrument selected surfaces with rows of static pressure tappings. The S nozzle, which was tested first, received this treatment. Sufficiently good agreement was obtained[11] between calculation and experiment in this, the more geometrically complex nozzle, to suggest that the lengthy process of instrumentation could be dispensed within the C variant.

It is noted that variations in the wall static pressure distributions of the two designs were essentially confined to the nozzles themselves; little difference was evident at the nominal exit plane. This finding, also mentioned by Boletis,[9] suggests that this type of wall contouring results in only minor changes to the radial static pressure distribution experienced at inlet to the rotor.

Increasing nozzle pressure ratio to the design value produced static pressure distributions on the vane suction surface and hub walls consistent with the presence of a significant shock system at nozzle exit. Some confirmation of this was provided by flow visualization, the results of which are shown in the photograph of Fig. 7. An oblique shock wave, emanating from the trailing edge of the adjacent vane, impinged on the uncovered suction surface. Further flow visualization, using an oil dot technique, suggested that although there was no clear separation line associated with the shock/boundary layer interaction, the hub/suction surface corner contained significant low momentum fluid which responded to the cross-channel pressure gradient at nozzle exit. Confirmation of this interpretation is provided by results of nozzle exit traverses. The flow visualization was used with both nozzles; only minor differences were apparent.

Radial Distribution of Losses at Nozzle Exit

As mentioned earlier, traversing was conducted at 11 circumferential positions spanning one vane pitch. Circumferential area averaging of total pressure losses at each radial immersion led to the mean radial distributions presented in Fig. 8 for nozzle C, covering a range of nozzle pressure ratio, *PR*, from subsonic (1.4) to supersonic (2.8). (Similar data for nozzle S are presented in Ref. 11.) Notwithstanding the thinner hub boundary layer at inlet, for all values of *PR* losses are substantially higher at the hub than at the tip. This arises from increased boundary layer growth in the adverse pressure gradient downstream of the throat (Fig. 3), as well as migration of vane surface boundary layers in response to the radial pressure gradient.

Under given flow conditions the highest Mach numbers occur in the freestream near the hub suction surface where local static pressures are the lowest, leading to maximum shock strength in that region. It is evident from data at 40 to 80% span that as the nozzle pressure ratio is increased above about 1.7 (representing the condition at which some local sonic flow is achieved), the shock/boundary layer interaction region on the vane suction surface extends farther toward the tip, leading to greater radial extent of the higher loss region.

It is interesting to note that in some regions near the hub the loss coefficients do not rise monotonically with increasing nozzle pressure ratio; the largest values are observed at the intermediate conditions. This may stem from the fact that at low-supersonic Mach numbers, the shock wave from the trailing edge of the adjacent vane impinges on the uncovered suction surface farther upstream than is the case at higher Mach numbers when the shock is more oblique. Although the shock/boundary layer interaction is a function

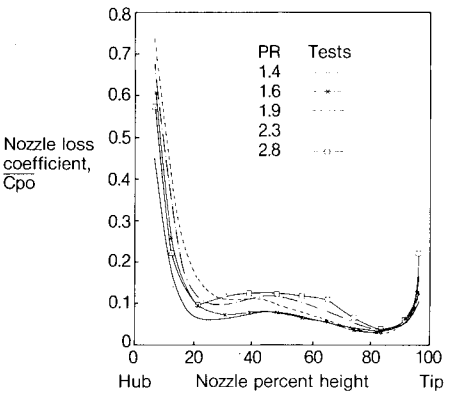

Fig. 8 Radial distribution of circumferentially averaged total pressure loss (nozzle C).

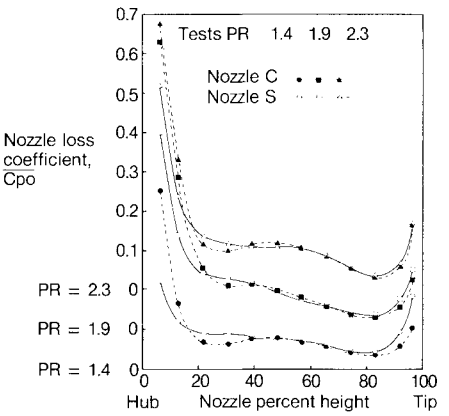

Fig. 9 Radial distribution of circumferentially averaged total pressure loss (comparison of nozzles C and S).

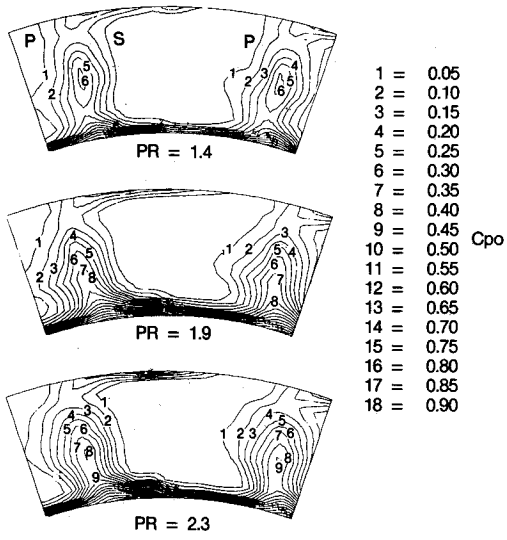

Fig. 10 Total pressure loss contours (nozzle C).

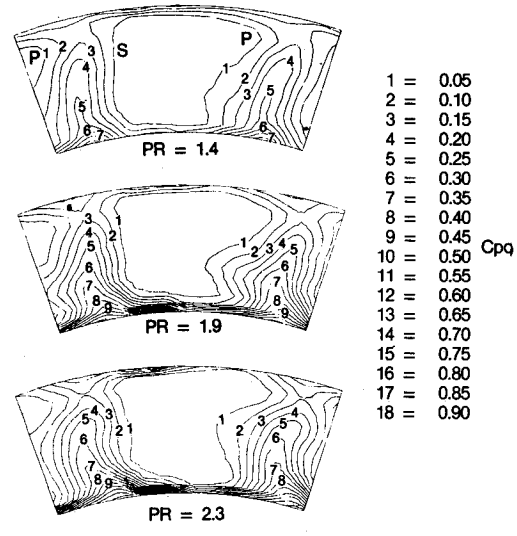

Fig. 11 Total pressure loss contours (nozzle S).

of shock strength, it may well be that the greater development distance of the disturbed boundary layer plays a significant role in determining the magnitude of the observed loss coefficients. An alternative explanation for similar behavior of loss coefficients in transonic flow was given by Graham and Kost[12] in a two-dimensional cascade test. Flow visualization by the schlieren method suggested that at low supersonic Mach numbers the shock system reflected from the suction surface was almost normal to the channel and did not lead to reattachment of the separating boundary layer. At higher Mach numbers the more oblique expansion wave reflected from the surface of the separation bubble was sufficient to force the boundary layer back toward the wall.

A comparison of the mean radial loss distributions of the two nozzle designs in Fig. 9 shows results at three values of *PR* corresponding to subsonic, transonic, and design conditions. (The vertical scales for the three nominal pressure ratios selected have been displaced for clarity.) It is immediately evident that near the hub significant reduction in total pressure loss was experienced by the S nozzle compared to the C variant. This probably reflects a weaker radial migration of the low-momentum flow from the inlet outer wall boundary layer. It also shows the differences in hub wall static pressure

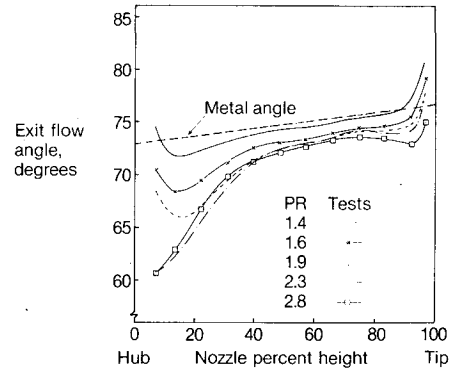

Fig. 12 Radial distribution of circumferentially averaged exit flow angle (nozzle C).

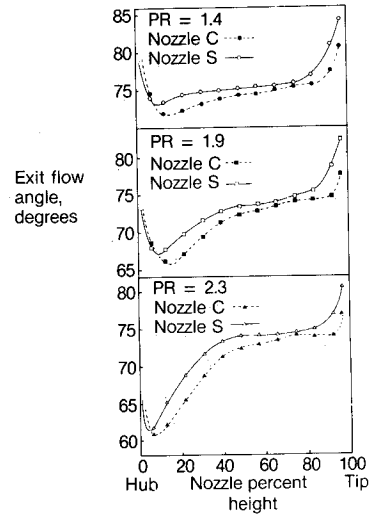

Fig. 13 Radial distribution of circumferentially averaged exit flow angle (comparison of nozzles C and S).

gradients near the exit, as noted earlier. The higher hub losses of the C nozzle were accompanied by a region of lower loss from 20 to 40% span; the two nozzles generally performed similarly from 40 to 70% span. In the tip region the S nozzle incurred higher losses when compared to the C variant. The unloading of the vane tip in the S nozzle (Fig. 4), while effective in reducing cross-channel flow, helped to retain low-momentum flow in the tip region where the subsequent adverse pressure gradient (noted in the discussion of Fig. 5) had a more deleterious effect.

Although the present results in the tip region are similar to those of Ref. 7, considerable differences are apparent near the hub, probably reflecting the difference in the vane loading, as well as detailed differences in the overall nozzle and contour design.

Total Pressure Loss Contours at Nozzle Exit

Three nominal values of nozzle pressure ratio *PR* (1.4, 1.9, and 2.3) have been selected to permit comparison of the two nozzle builds from subsonic to supersonic exit conditions in terms of contours of total pressure loss coefficients Cp_o (Figs. 10 and 11). As noted earlier, measurements were taken over a circumferential distance corresponding to one vane pitch. For clarity of presentation the pattern of measurements has been partially repeated to cover more than a single vane pitch and show the repetitive wake effect. Hub and tip regions are truncated in these plots which cover only the approximate radial extent of the traverse measurements, from 4 to 96% span.

Essentially radial regions of loss corresponding to vane wakes are evident in these figures. The characteristics of the wakes are broadly similar for the two nozzle designs and clearly a function of nozzle pressure ratio. The increase in three-dimensionality of the wake under transonic conditions ($PR = 1.9$) when compared to the subsonic case ($PR = 1.4$) is clear for both nozzles, together with the increase in magnitude of the hub loss region associated with the shock/boundary layer interaction. The supersonic exit condition ($PR = 2.3$) shows a movement of the maximum wake thickness toward the tip, perhaps associated with the position of transonic conditions at the vane trailing edge. It also illustrates the slight reduction in the extent of the hub loss region noted earlier.

In comparison to the S nozzle results, the increased radial extent of the hub loss region, and corresponding decreased radial extent of the tip loss region of the C nozzle (noted in the discussion of Fig. 9), are evident throughout the pressure ratio range. The contour plots, however, permit a more detailed assessment of nozzle performance; thus attention is directed particularly to the tip wall/pressure surface intersection which shows distinct differences between nozzle builds. The S nozzle, with its reduced cross-channel and radial static pressure gradients, shows a more nearly symmetric wake at the vane/endwall intersection, whereas at the tip of nozzle C, the endwall boundary-layer flow is swept toward the suction surface by the cross-channel static pressure gradient, resulting in an asymmetric vane wake near the tip.

Radial Distribution of Flow Angle at Nozzle Exit

Circumferentially averaged values of exit flow angles from nozzle C are presented in Fig. 12 for values of pressure ratio PR from 1.4 to 2.8. (Similar data for nozzle S are presented in Ref. 11.) At low-pressure ratio a classical secondary flow pattern involving slight underturning over most of the span and overturning near the walls is obtained. Increase in pressure ratio lowers the general level of turning and results in development of a region of significant underturning near the hub wall. At supersonic exit conditions this region continues to intensify and moves nearer the hub wall, as noted in the earlier discussion of the loss distributions. Intensification of the tip vortex is also evident under these conditions.

Comparison of the flow turning performance of the two nozzles is afforded by Fig. 13. It is apparent that over most of the central part of the span the S nozzle shows greater flow turning than the C version (although approximately 0.7 deg of this is due to the restagger noted earlier). Near the tip the radial extent and magnitude of the S nozzle overturning is significantly greater than in the C variant, associated with the increased secondary flow in that region seen in Fig. 9. The corresponding reduction in radial extent of the low-turning hub region of the S nozzle is also clearly shown.

Assessment of Overall Performance

Measured values of total pressure at nozzle exit were combined with linearly interpolated values of static pressure (derived from mean hub and tip values) to yield local values of Mach number. Overall area weighted averaging of these values was then employed to derive the mean exit Mach number, the parameter used in this section to characterize nozzle flow conditions.

Area weighted averaging of the mean radial distributions of total pressure loss coefficients and flow angles measured at nozzle exit permitted overall performance to be assessed for the various test conditions (Fig. 14). As a point of interest an attempt was made to use mass flow weighted averaging, but check calculations against measured mass flow were unsatisfactory. Accuracy of mass flow weighting in flows such as these requires use of appropriate local values of static pressure, rather than overall mean interpolated values. Also, knowledge of local flow angles assumes considerable importance (1 deg error in a flow angle of 76 deg incurs a 7% error in mass flow).

Area weighted overall mean flow angles (Fig. 14) are seen to decrease monotonically for both geometries with increasing mean exit Mach number. The major part of the reduction occurs shortly after the onset of local supersonic flow in the nozzles. At the low exit Mach number the difference between the two nozzles is almost accounted for by the difference in stagger angle (0.72 deg) of the two builds. It appears that at design Mach number, the flow deviation from the conical nozzle is increased by slightly more than 1 deg compared to nozzle S.

Overall mean total pressure losses are nondimensionalized in three different ways. Referencing to the nominally constant upstream total pressure, Pom_1, (to give loss coefficient Yp) permits presentation of the trend in absolute total pressure loss with increasing nozzle pressure ratio. Again the relationship with mean exit Mach number is monotonic. The most marked increase in loss occurs with transonic flow due to shock/boundary layer interactions at the hub walls. Nozzle C shows higher losses throughout the Mach number range and, probably due to its larger hub loss, incurs a

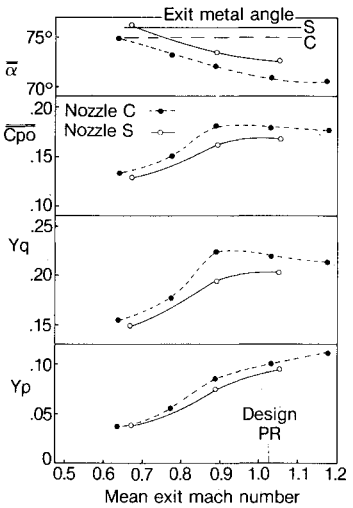

Fig. 14 Effect of exit Mach number on nozzle performance parameters.

Table 1 Numerical values of the overall measured performance parameters

Nominal PR	1.4		1.6	1.9		2.3 (design)		2.8
Nozzle	S	C	C	S	C	S	C	C
Mean exit Mach number	0.670	0.638	0.775	0.890	0.889	1.053	1.030	1.183
$\bar{\alpha}$ (deg)	76.2	75.0	73.3	73.5	72.1	72.7	70.9	70.7
$\overline{Yp}$	0.039	0.037	0.058	0.075	0.086	0.096	0.101	0.113
$\overline{Cp_o}$	0.129	0.133	0.150	0.161	0.182	0.168	0.179	0.175
Yq	0.150	0.155	0.179	0.195	0.224	0.204	0.220	0.214

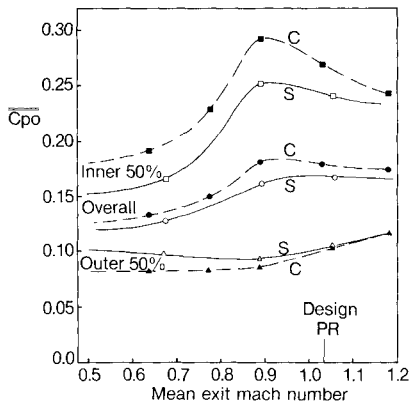

Fig. 15 Effect of mean exit Mach number on inner and outer annulus loss split.

greater penalty with the onset of shock/boundary interactions in that region.

Loss coefficient Yq, based on the area weighted mean of measured total to static pressure differences at nozzle exit plane, has been used as a performance parameter in some earlier studies and shows much the same trend with Mach number as the loss coefficient $\overline{CP}_o$. In both cases, the initial transonic rise in loss coefficient is followed by a slight reduction at higher Mach numbers as the absolute rise in losses is more than offset by the increasing value of the normalizing parameter (exit dynamic pressure). Again, the differences between the two nozzle designs are only slightly affected by exit Mach number. For reference, numerical values of the overall measured performance parameters are summarized in Table 1.

The effect of contour geometry and exit Mach number on the loss split between the inner and outer 50% of the annulus is presented in Fig. 15 in terms of $\overline{CP}_o$. For both nozzle designs it is again apparent that it is the hub loss associated with the onset of shock/boundary layer interaction which contributes to the transonic loss peak evident in the overall performance. Losses in the outer half of the annulus are relatively insensitive to Mach number, reflecting the late onset of transonic flow in this region. Retention of low momentum flow in the tip region of nozzle S by reduction of the cross-channel pressure gradient appears to minimize radial migration on the vane suction surface compared to nozzle C and reduces the losses in the more critical hub area. The higher loss of nozzle S in the outer half of the annulus is thus more than offset by the corresponding reduction in hub loss.

The present work has shown that degradation of overall performance with increasing Mach number was dominated by the growth of high losses and flow underturning near the hub. Subsequent tests[11] have measured the downstream development of this region of incipient separation and have indicated rapid growth to occur beyond the nozzle exit plane. Current work with a representative rotor in place behind the nozzle suggests that, although wall static pressures at the nominal nozzle exit plane are essentially unaffected, the modification due to the rotor of the flow field downstream of the nozzle exit may have some beneficial impact on measured nozzle performance. The work is continuing and will be published at a later date.

Conclusion

As would be expected, there were a number of similarities in the general aerodynamic behavior of the two nozzle designs. Both showed significant modification of total pressure losses and of secondary flow development with the appearance of a shock system near the hub wall at exit. As Mach number was increased, development of shock/boundary layer interactions promoted boundary-layer growth in the vicinity of the hub/suction surface intersection and led to a rapid increase in three-dimensional effects and losses. Mean flow deviation angle and absolute values of total pressure losses were observed to rise monotonically with exit Mach number, the sharpest increase occurring in transonic flow.

The most obvious difference in the performance of the two nozzle builds was the significantly greater hub total pressure loss at exit of the C nozzle compared with the S variant. This difference, not offset by the corresponding decrease in tip losses, led to higher overall total pressure losses for the C nozzle throughout the test range of Mach number. The thicker hub loss region at the C nozzle exit, associated with increased secondary flow, led to a greater flow deviation angle at transonic and higher Mach numbers than was experienced by the S variant.

Current work, to be reported shortly, suggests that the region of incipient separation at the hub (and the associated effects on total pressure losses and flow angle) may be beneficially affected by the presence of an operating rotor at nozzle exit.

Acknowledgments

The work reported herein is part of a joint research program carried out by the National Research Council of Canada (NRC), and Pratt and Whitney Canada Inc. (P&WC). Contributions by Ü. Okapuu, S. C. Kacker, and J.-P. Huot of P&WC, together with NRC assistance from B. J. Day an D. Logan are gratefully acknowledged.

References

[1]Deich, M. E. et al., "Method of Increasing the Efficiency of Turbine Stages with Short Blades," Translation No. 2816, Associated Electrical Industries, Ltd., Manchester, England, April 1960.

[2]Morris, A.W.H. and Hoare, R. G., "Secondary Loss Measurements in a Cascade of Turbine Blades with Meridional Wall Profiling," ASME Paper 75-WA/GT-13, Nov. 1975.

[3]Ewen, J. S., Huber, F. W., and Mitchell, J. P., "Investigation of the Aerodynamic Performance of Small Axial Turbines," ASME Paper 73-GT-3, April 1973.

[4]Okapuu, Ü., "Some Results from Tests on a High Work Axial Gas Generator Turbine," ASME Paper 74-GT-81, March 1974.

[5]Kopper, F. C., Milano, R., and Vanco, M., "An Experimental Investigation of Endwalls Profiling in a Turbine Vane Cascade," AIAA Paper 80-1089, June 1980.

[6]Boyle, R. J. and Haas, J. E., "Comparison of Experimental and Analytical Performance for Contoured Endwall Stators," AIAA Paper 82-1286, June 1982.

[7]Haas, J. E., "Analytical and Experimental Investigation of Stator Endwall Contouring in a Small Axial-Flow Turbine. 1—Stator Performance," NASA TP-2023, 1982.

[8]Haas, J. E. and Boyle, R. J., "Analytical and Experimental Investigation of Stator Endwall Contouring in a Small Axial-Flow Turbine," NASA TP-2309, 1984.

[9]Boletis, E., "Effects of Tip Endwall Contouring on the Three-Dimensional Flow Field in an Annular Turbine Nozzle Guide Vane: Part I—Experimental Investigation," ASME Paper 85-GT-71.

[10]Denton, J. D., "A Time Marching Method for Two- and Three-Dimensional Blade to Blade Flow," ARC R&M 3775, 1975.

[11]Williamson, R. G. and Moustapha, S. H., "Three-Dimensional Cascade Testing of Turbine Nozzles at High Exit Mach Numbers," *Three-Dimensional Flow Phenomena in Fluid Machinery*, ASME FED, Vol. 32, Nov. 1985.

[12]Graham, C. G. and Kost, F. H., "Shock Boundary Layer interaction on High Turning Transonic Turbine Cascades," ASME Paper 79-GT-37, March 1979.